Research Square

Preprints are preliminary reports that have not undergone peer review.
They should not be considered conclusive, used to inform clinical practice,
or referenced by the media as validated information.

Automated Penetration Testing for Static Yield Stress and Structural Build-Up in 3D Concrete Printing: Accuracy Across SCM and Fiber-Reinforced Mixtures

Shiva Kumar Goud Kasani
Missouri University of Science and Technology
Ali Fasihi
Missouri University of Science and Technology
Nicolas A. Libre
libren@mst.edu

Missouri University of Science and Technology

Research Article

Keywords: Static yield stress, Structural build-up, Penetration probe, Vane rheometry, 3D concrete printing (3DCP)

Posted Date: November 23rd, 2026

DOI: https://doi.org/10.21203/rs.3.rs-11589398/v1

License: This work is licensed under a Creative Commons Attribution 4.0 International License.
Read Full License

Additional Declarations: No competing interests reported.

Automated Penetration Testing for Static Yield Stress and Structural Build-Up in 3D Concrete Printing: Accuracy Across SCM and Fiber-Reinforced Mixtures

Shiva Kumar Goud Kasani, Ali Fasihi, Nicolas A. Libre*
Department of Civil, Architectural and Environmental Engineering, Missouri University of Science and Technology, Rolla, MO, USA
libren@mst.edu

Abstract

Controlling buildability in modern printable mixtures requires rapid, frequent yield stress (τ_0) measurements that traditional laboratory rheometers cannot deliver on-site. Penetration methods provide a viable on-site alternative. However, whether they remain accurate across the expanding range of printing materials with various supplementary cementitious materials (SCMs), and fiber-reinforcement remains an open question. This study evaluated an automated, displacement-controlled penetration method that interprets the complete force–displacement response using tip and full penetration procedures, on 18 printable mortars spanning two cement types, four SCMs (fly ash, silica fume, calcined clay, limestone filler), and three fiber types (polypropylene, steel, hemp) at multiple dosages. Vane rheometer, tip penetration, full penetration, and mini-slump tests were performed simultaneously on identical batches at six material ages (n = 103), separating systematic bias from random scatter. Both penetration methods tracked the rheometer τ_0 with high precision ($R^2 = 0.90$). Full penetration reproduced the rheometer τ_0 value with a near-unity slope (1.07), whereas tip penetration overestimated it by 27% on average, rising to twofold for silica fume and steel-fiber mixtures. At high fiber dosages, the sensitivity of full penetration to τ_0 was substantially reduced (steel) or not statistically resolvable (polypropylene), while tip penetration retained a stable, correctable bias; hemp mixtures remained compatible with both methods at all

dosages. For the structural build-up rate, the ranking reversed: full penetration reproduced the rheometer-derived rate (median deviation 16% in fiber mixtures) whereas tip penetration overestimated it (45%). Class-specific conversion factors and a selection framework matching penetration method to material class and quantity of interest are provided.

Keywords: *Static yield stress, Structural build-up, Penetration probe, Vane rheometry, 3D concrete printing (3DCP)*

1. Introduction

During the past ten years, the 3D concrete printing (3DCP) materials have evolved significantly from simple cementitious pastes into complex, multi-component systems. Driven by decarbonization targets, printable binders are increasingly adopting high replacement levels of supplementary cementitious materials (SCMs) such as fly ash, silica fume, limestone filler and calcined clay [1-4]. In addition, since conventional reinforcement cannot be easily incorporated into layer-wise deposition, short fibers such as polypropylene, steel, and more recently natural fibers such as hemp, have become routine constituents of printable mixtures [4-7]. These constituents are not inert additives: they influence water demand, particle packing, and flocculation kinetics. In particular, in fiber reinforced mixtures, fibers form a reinforcing network in the fresh paste, that modifies the fresh-state rheology with the magnitude of these effects depending strongly on fiber type and dosage [8-11]. The mixtures being printed today are therefore very different from those on which the field's fresh-state test methods were originally developed.

Static yield stress (τ_0) is the rheological parameter that governs whether a deposited layer retains its geometry and carries subsequent layers without collapse [12-14]. Because τ_0 evolves continuously at early ages through flocculation and early hydration, the printability windows are

narrow [15-17]. The τ_0 must be tested and monitored frequently during the printing process to ensure the material stays within its printability window as it is being deposited. Rotational and vane rheometers remain the reference for τ_0 and produce reliable values under controlled conditions [18], but they are bench-mounted laboratory instruments, operator-dependent, and slow relative to the pace at which fresh-state properties change on site. This mismatch has motivated researchers to develop rapid, portable, automatable methods capable of measuring τ_0 frequently enough to support quality control and, ultimately, feedback control of the printing process [19,20].

Penetration testing has been used for characterizing fresh properties of concrete, but the term covers a wide family of test procedures that should not be confused with each other. Constant-load approaches such as the Vicat needle and the fall cone record penetration depth under a fixed load [21,22]; quasi-static penetrometers [23,24], sheet indenters [25], and hand-held probes [26] differ in probe geometry, penetration rate, and submergence depth. These penetration test methods usually reduce the material response to a single scalar such as a maximum force, a depth, or a force at a prescribed depth. A distinct class of procedure has since emerged: automated, displacement-controlled penetration, in which a probe of defined geometry advances at constant speed while the complete force–displacement response is recorded and interpreted, rather than a single extracted value [27,28]. Two configurations of this approach have been established, each with a theoretical basis for conversion to τ_0: full penetration, in which the probe is fully submerged and the yield force is identified from the developed force–displacement curve [29]; and tip penetration, in which yielding is identified from an equilibrium penetration stress at shallow depth, without requiring full submergence, making it compatible with thin printed filaments and shorter test durations [30]. Both have shown a strong correlation with the vane rheometer on baseline cementitious systems, and both have demonstrated sensitivity to structural build-up over time [29,30].

The performance of these test methods in more complex mixtures requires further investigation. While the accuracy of these penetration methods is established for baseline systems, their domain of validity across the increasing material complexity of modern printable mixtures, particularly fiber-reinforced systems has not been systematically evaluated. Consequently, no clear guidance currently exists regarding which penetration mode is optimal for specific material classes. Individual studies have applied penetration-type methods to mixtures containing SCMs and chemical admixtures [31,32], and each reports a correlation with a reference method for its own material set. But these studies differ in device, probe geometry, penetration rate, and reference technique, and each pools its mixtures into a single correlation. As a result, three questions remain unanswered under a single protocol and a common reference: (i) whether and at what dosage specific constituent classes degrade the accuracy of penetration-derived τ_0; (ii) whether fiber reinforcement, which is increasingly becoming common in 3DCP and yet has a very limited validation record, compromises the penetration test results. This question is sharpened by the fact that the reference rheometer methods themselves are known to be sensitive in high fiber mixtures [11]; and (iii) how the tip and full configurations compare when applied to identical materials at identical ages [30]. Answering these questions requires a design that includes penetration, reference rheometer, and empirical workability tests performed simultaneously on the same batches, at the same material ages, across mixtures spanning the constituent space of common printable concrete materials.

This study addresses these questions through a comprehensive experimental program. Eighteen printable mortar mixtures were studied, including two cement types (Type I and Type III), four SCMs (fly ash, silica fume, calcined clay, limestone filler), and three fiber types (polypropylene, steel, hemp) at two dosages each for polypropylene and steel fibers and three dosages for hemp

fiber. For every mixture, τ_0 was measured at six material ages using four methods on the same batch: vane rheometer (reference method), tip penetration, full penetration, and mini-slump tests. The objectives were to determine: (i) whether the two penetration configurations retain accuracy against vane rheometer across SCM-modified mixtures; (ii) whether they retain accuracy and robustness in fiber-reinforced mixtures, and at what fiber type and dosage each configuration breaks down; (iii) what systematic bias exists between methods, whether that bias is constituent-dependent, and to what extent it can be corrected; and (iv) whether both configurations track the rate of structural build-up, and whether the configuration best suited to τ_0 magnitude is also best suited to its rate. All measurements were performed on mold-cast specimens under laboratory conditions; evaluation on deposited filaments during printing is identified as the necessary next step and is outside the present scope.

2. Materials and methods

2.1 Materials

The mixtures were formulated using locally sourced aggregate and two types of ordinary Portland cement (OPC) compliant with ASTM C150 [33]: Type I/II and Type III. The cement's chemical composition, analyzed through X-ray fluorescence spectrometry, is presented in Table 1. The Type I/II cement's specific surface area, specific gravity, and loss on ignition were measured as 390 m^2/kg, 3.14, and 1.5% by weight, respectively. Type III cement's specific surface area, specific gravity, and loss on ignition were measured as 588.3 m^2/kg, 3.17, and 1.81% by weight, respectively. The aggregate characteristics included a nominal maximum size of 2 mm, a fineness modulus of 3.69, a specific gravity of 2.58, and an absorption rate of 2.01%. The particle size distributions of the cement, SCMs (fly ash, silica fume, calcined clay, and limestone filler) and aggregate are illustrated in Figure 1. The SCMs included fly ash, silica fume, calcined clay, and

limestone filler. The fly ash, silica fume, and calcined clay conformed to ASTM C618 [34]; limestone filler is not covered by this standard. A polycarboxylate-based superplasticizer (SP) with a solid content of 23% and a specific gravity of 1.05 (Master Glenium 7500) was employed to increase workability. The cellulose-based viscosity-modifying admixture (VMA) with a SP/VMA weight-ratio of 1.3 was introduced to the mixes with type III cement. Three types of fibers, namely polypropylene (synthetic), steel (rigid) and hemp (natural) fibers were introduced into type I mixtures. The physical characteristics of these fibers are summarized in Table 2. Hemp fiber was pre-treated before use, to remove surface impurities and improve interfacial bonding with the cementitious matrix [35,36]. First, fiber was washed with distilled water to remove dirt, then oven dried for 6 h at 60 °C. After drying, fibers were soaked for 15 h in 5 wt% NaOH solution. After removal from the NaOH solution, fibers were rinsed with distilled water, then with a diluted white vinegar solution to neutralize residual alkalinity and rinsed once more with distilled water before being dried at 60 °C for 6 h [37].

Table 1 Chemical composition of raw materials

	SiO_2, %	Al_2O_3, %	Fe_2O_3, %	CaO, %	MgO, %	Na_2O eq, %	K_2O, %
Type I cement	18.7	4	3.6	65.9	1.7	0.97	-
Type III cement	19.56	4.72	2.63	62.53	3.38	0.66	-
Fly ash	40.64	21.09	5.68	20.6	4.42	2.26	0.78
Silica fume	95.5	0.7	0.3	0.4	0.5	0.4	-
Calcined clay	57.1	35.3	3.3	0.73	0.68	-	1.04
Limestone	2.97	0.7	0.17	95.33	0.18	-	0.13

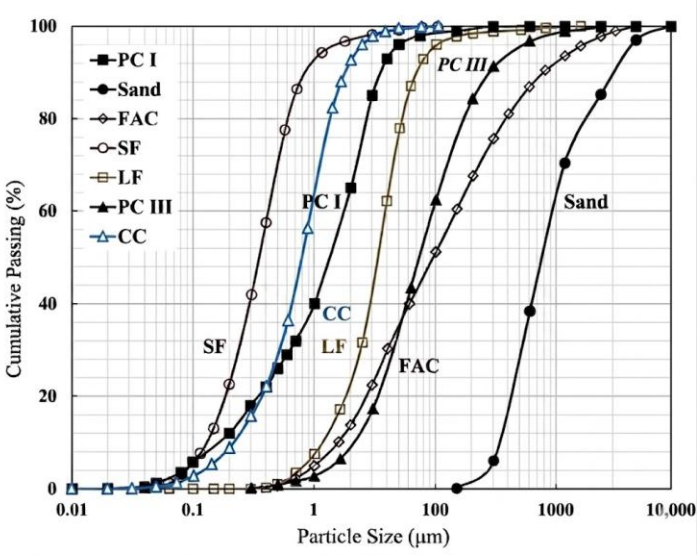

Fig. 1 Particle distribution of cement, sand, fly ash, silica fume, calcined clay and limestone filler

Table 2 Physical characteristics of polypropylene, steel and hemp fibers

Fiber type	Length (L): mm	Diameter (d): mm	Aspect ratio	Tensile strength (MPa)	Elastic modulus (GPa)
Polypropylene	8	0.038	210	1600	40
Steel	6	0.2	30	2100	154
Hemp	12	0.5	24	550-900	30-70

2.2 Mix proportions and mixing procedure

Mixture proportions were designed based on formulations reported in the 3DCP literature, with SCM replacement levels and fiber dosages selected to represent the most commonly used or optimum values reported for successful printing [37-39]. A water-to-cement ratio (w/c) of 0.30 and a sand-to-binder (s/b) ratio of 1.0 were held constant across all mixtures. The eighteen mixtures comprise a plain reference mixture for each cement type; single and combined SCM replacements fly ash, silica fume, calcined clay, and limestone filler, with and without a VMA; and fiber-reinforced mixtures at two dosages each for polypropylene and steel fibers and three dosages for hemp fiber. Full proportions for all 18 mixtures are given in Table 3.

All measurements were conducted over a 60-minute period, with data recorded at 10, 20, 30, 40, 50, and 60 minutes from the time of mixing. Dry ingredients (cement, SCMs, and fine aggregate) were mixed in a 30-quart Hobart mixer at low speed for 3 minutes to ensure uniform binder–aggregate distribution. Ninety percent of the mixing water was then added and mixed at low speed for 3 minutes; the remaining 10%, pre-blended with the SP, was added gradually at low speed, with the sides and bottom of the mixing bowl scraped periodically to ensure homogeneity. Mixing speed was then increased to medium for 2 minutes until a uniform, workable consistency was achieved. For fiber-reinforced mixtures, fibers gradually dispersed over 2 minutes under continuous low-speed mixing to prevent balling. This process was repeated two to three times depending on fiber dosage and was followed by 2 minutes of medium-speed mixing until visual inspection confirmed uniform dispersion with no dry pockets. The fresh mix was then cast into molds for concurrent testing.

Table 3 Mixture proportion of the tested mixtures

Class	Mix code	Cement (kg/m³)	Aggregate (kg/m³)	SCM (kg/m³)	Water (kg/m³)	SP (%)	VMA (%)	Fiber (%vol)	Fibers mean spacing (mm) Eq. (2)	Ref
baseline mixtures	Control	991	991	–	304.2	0.37	–	–	–	[38]
	30FA	672	960	288 FA	294.8	0.36	–	–	–	[38]
	30FA_15SF	502.8	914	274 FA + 137 SF	280.7	0.54	–	–	–	[38]
	5SF	925	974	48 SF	299.1	0.40	–	–	–	[-]
	10SF	862	957	95.8 SF	294.1	0.44	–	–	–	[-]
	15LF	800	942	141 LF	289.2	0.20	–	–	–	[-]
Accelerated/structuring binders	CIII	991*	991	–	304.2	0.54	–	–	–	[-]
	20CC	776*	970	194 CC	297.9	0.46	–	–	–	[-]
	20CC_15LF	600*	923.30	184 CC+ 138.50 LF	283.5	0.83	–	–	–	[-]
	20CC_VMA	776*	970	194 CC	297.9	0.80	0.58	–	–	[-]
	30CC_15LF_VMA	482*	876	262 CC+ 131 LF	268.9	0.64	0.48	–	–	[39]
Fiber-reinforced mixtures	ST_L	502.8	914	274 FA + 137 SF	280.7	0.48	–	0.75 steel	2.05	[38]
	ST_H	502.8	914	274 FA + 137 SF	280.7	0.48	–	1.5 steel	1.45	[38]
	PP_L	672	960	288 FA	294.8	0.37	–	0.375 PP	0.55	[38]
	PP_H	672	960	288 FA	294.8	0.44	–	0.75 PP	0.39	[38]
	HF_L	925	974	48 SF	299.1	0.51	–	0.375 hemp	7.24	[37]
	HF_M	925	974	48 SF	299.1	0.54	–	0.75 hemp	5.12	[37]
	HF_H	925	974	48 SF	299.1	1.81	–	1.5 hemp	3.62	[-]

Note: *Abbreviations used in the table are as follows: C: type I OPC; C* = type III OPC; FA = fly ash; SF = silica fume; LF = limestone filler; CC = calcined clay; PP = polypropylene fiber; ST = steel fiber; HF = Hemp fiber; L = low, M = medium, and H = high fiber volume. Fiber content is expressed as a percentage of total mixture volume, and superplasticizer (SP) dosage is expressed as a percentage of total binder weight. VMA dosages is expressed as a percentage of total binder weight. The water-to-cement ratio (w/c) and sand-to-binder ratio (s/b) were held constant at 0.30 and 1.0, respectively, across all mixtures. A dash (−) indicates that the respective constituent was not incorporated in the mixture. Reference numbers correspond to the source mix designs from which the proportions were adapted. Mixtures marked [-] in the Ref column were developed in the present study.

2.3 Test methods

All measurements were conducted over a 60-minute time period, with data recorded at 10, 20, 30, 40, 50, and 60 minutes from the time of mixing. The monitoring was initiated at 10 minutes rather than immediately after mixing to allow sufficient time for sample preparation and mold filling. Six cylindrical molds were prepared for the vane rheometer test, and three square molds were prepared simultaneously after the time of mixing as shown in Figure 2, each filled in two layers and compacted by 7 taps for vane and 14 tamps per layer using a rod to ensure uniform sample density across all specimens. Molds not under active testing were sealed with plastic wrap to prevent moisture loss until their respective measurement interval. At each time interval, tip penetration, full penetration, vane rheometer, and mini-slump tests were conducted simultaneously on the same batch, ensuring all measurements reflected identical material age and curing conditions.

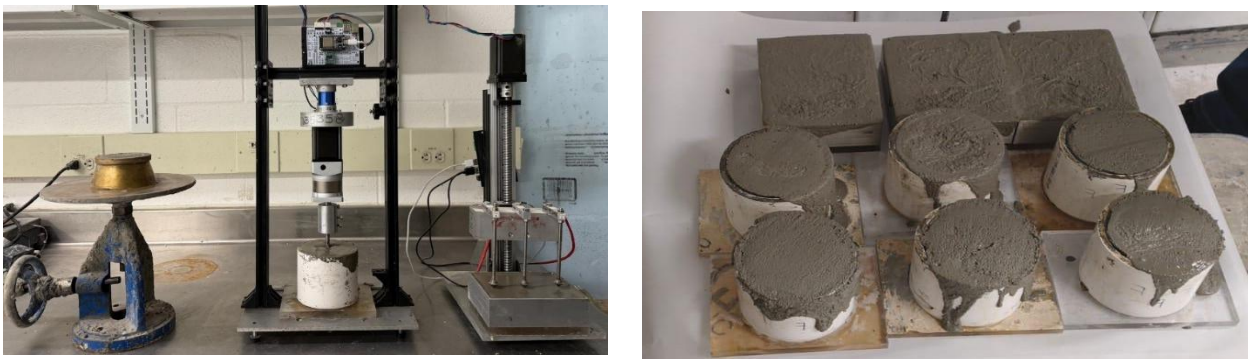

Fig. 2 Experimental setup used in this study: (a) slump flow, vane rheometer, and automated penetration testing; and (b) concrete samples prepared for testing at different ages

2.3.1 Penetration test

An automated penetration device with three independent probes [29] was used, allowing parallel testing within the same time interval. Stainless steel, mirror-polished cones with semi-angle (β) = 45° and base diameter 20 mm were used, driven at a constant displacement speed of 1 mm/s. The experimental setup for the tip and full penetration tests is shown in Figure 3. Each probe recorded two readings in sequence on the same insertion: a tip penetration reading at shallow depth, and a full penetration reading once fully submerged. The two are acquired a few seconds apart on the same specimen: the probe advances to 25 mm and the tip penetration reading is taken; the probe then stops, the load cell is re-zeroed, and the full penetration reading is acquired as the probe resumes advancing under the same displacement control. The tip and full penetration readings therefore come from one penetration sequence at one location, rather than from separate tests requiring a new specimen or a change of instrument.

Tip penetration: Force and displacement are recorded as the cone advances to 25 mm depth, and penetration stress is calculated by dividing force by the cone contact area, following the procedure of Fasihi et al. [30].

Full penetration: After the tip penetration reading and re-zeroing, the probe continues at the same speed until fully submerged. The force–displacement curve is recorded, and the yielding force is identified as the peak force within 6 mm of the onset of the zeroed record, following the same procedure. The yielding force from the three probes is averaged and converted to τ_0 using the procedure of Fasihi et al. [29].

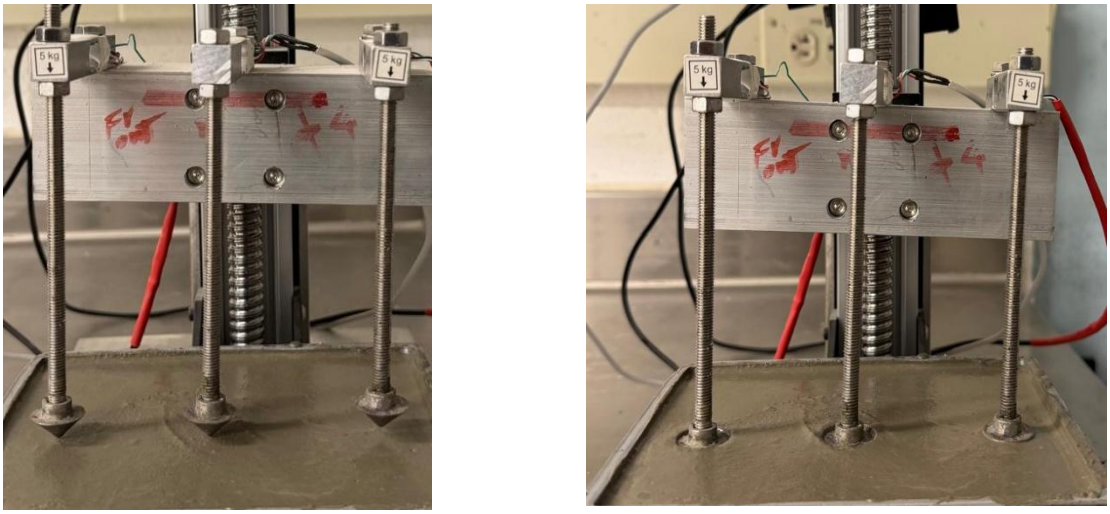

Fig. 3 The tip penetration probe test: (a) and the full penetration probe test: (b) positioned above the fresh cementitious mixture surface prior to testing

2.3.2 Mini slump test

Mortar flowability was evaluated using a flow table test in compliance with ASTM C1437 [40]. The test utilized a cone with a bottom diameter of 100 mm, an upper diameter of 70 mm, and a height of 50 mm. The slump flow was determined by averaging the maximum and minimum diameters of the mortar spread following 25 cycles of jolting.

2.3.3 Vane rheometer test

The τ_0 was measured using a four-bladed vane rheometer with a 50 mm diameter and height as the primary reference for all mixtures. Six cylinders were cast immediately after mixing and were sealed to prevent evaporation. Tests were conducted at specified intervals at 0.2 rpm, and torque (T_m) data were recorded. All vane rheometer tests were conducted simultaneously with tip penetration, full penetration, and mini-slump tests at each interval, ensuring all measurements reflected identical material age. τ_0 was then calculated as:

$$\tau_0 = \frac{12T_m}{\pi {D_v}^2 (6H_v + D_v)} \quad \text{Eq. (1)}$$

where D_v and H_v are the vane diameter and height [41].

2.4 Data Analysis

Agreement between each penetration configuration and the vane rheometer reference was evaluated by ordinary least-squares regression of the penetration-derived τ_0 against the simultaneously measured vane τ_0, with a free intercept. Evaluating this agreement requires distinguishing two failure modes of a measurement method: systematic deviation from the reference and random scatter about it [42]. Following ISO 5725-1, the systematic component is referred to here as trueness, quantified by the regression slope, and the random component as precision, quantified by R^2; accuracy denotes their combination. Trueness and precision are independent properties and are evaluated separately throughout.

ISO 5725-1 expresses bias as an additive offset at a stated level. Because the deviation between methods was found here to be proportional rather than additive (Section 3.3), trueness is quantified as proportional bias obtained from the regression slope, and the corresponding limits of agreement are reported as multiplicative factors.

Confidence intervals for the class-level regression slopes and all R^2 values were obtained by percentile bootstrap resampling of mixture–age pairs (1000 resamples, 2.5th and 97.5th percentiles), which assumes no particular error distribution and accommodates the unequal class sizes. A fixed random seed was used so that the reported intervals are exactly reproducible. Confidence intervals for the pooled slopes reported in Section 3.1 are analytical 95 % t-intervals obtained from ordinary least-squares estimation. Agreement was further assessed by Bland–Altman analysis, with proportional bias tested by regressing the paired difference against the paired mean ($\alpha = 0.05$). Material classes were designated quantitative (Q) where $n \geq 10$, $R^2 \geq 0.80$ and

the slope confidence interval excluded zero; indicative (I) where n < 10; and not convertible (NC) where the slope confidence interval included zero.

3. Results and discussion

3.1 Measurement performance across the entire mixture matrix

The applicability of the penetration method to modern printable mixtures which incorporate diverse binders, fibers, and admixtures depends fundamentally on its ability to accurately measure τ_0 across the entire experimental dataset. Figure 4 addresses this condition by comparing penetration-derived τ_0 with the τ_0 derived from vane rheometer as the standard test method across all 18 mixtures at six testing ages (n = 103); five mixture–age data points lacked a valid vane rheometer measurement due to the high stiffness of the mixtures and were excluded from this analysis. All methods were performed simultaneously at the same time on the same batch; therefore the difference observed in these figures is attributed to the test methods themselves rather than to differences in material state.

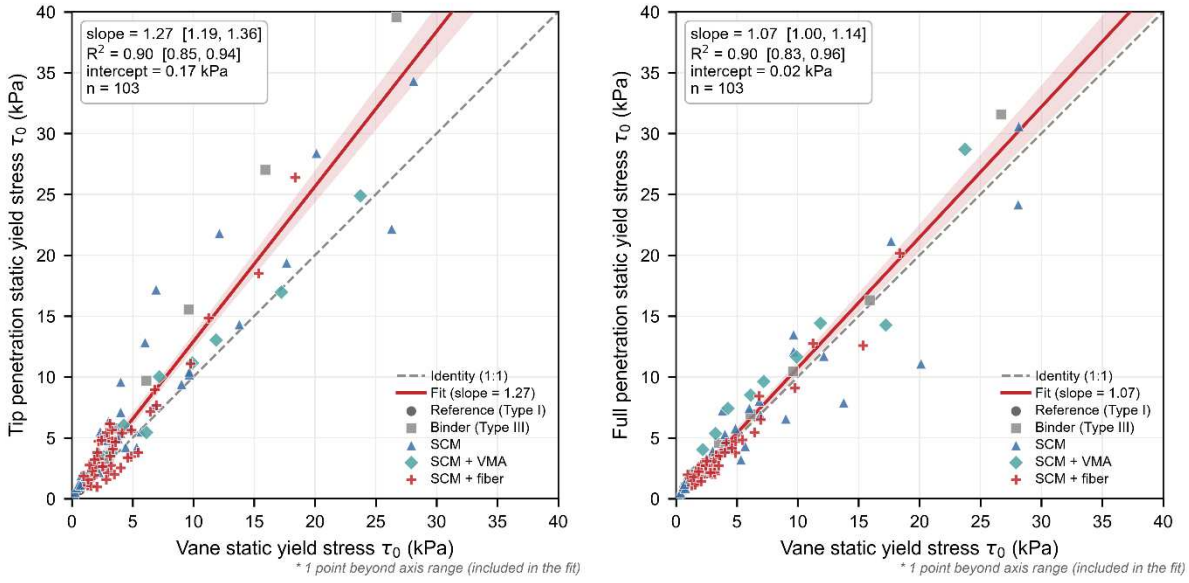

Fig. 4 Variation between the τ_0 derived from vane rheometer: (a) tip penetration; and (b) full penetration test configuration

Accuracy, trueness and precision: Both graphs in Figure 4 include the identity line and the 95% confidence interval (CI) of the fit which denotes the range within which the true regression line is expected to fall with 95% confidence. The full penetration and the tip penetration tests differ mainly in the trueness (regression slope) but not in the precision (R^2, data scatter). The full penetration configuration reproduces rheometer τ_0 with near-unity proportional bias: the regression slope is 1.07 (95% CI 1.00–1.14), marginally above unity, with a negligible intercept (0.02 kPa). The tip configuration, by contrast, overestimates τ_0 systematically: its regression slope of 1.27 (95% CI 1.19–1.36) corresponds to an average overestimation of approximately 27%, with a 95% CI that lies entirely above unity, confirming the overestimation is systematic rather than a sampling artifact. In terms of precision, however, the configurations are statistically indistinguishable, with $R^2 = 0.90$ for both (95% CI 0.83–0.96 for full; 0.85–0.94 for tip). Both configurations thus track changes in τ_0 with comparable precision, while only the full penetration method reports its magnitude without correction.

This result has a methodological implication for how the robustness of the method should be assessed. Correlation with a reference method is the most commonly reported evidence of validity in penetration studies, yet by that criterion alone the two configurations would appear equivalent here despite a 20-percentage-point difference in proportional bias. In other words, the regression slope must be reported and evaluated independently of R^2 when validating a test performance.

The τ_0 is a method-dependent quantity with no single true value; the τ_0 obtained from the vane rheometer is adopted here as the reference because the rheometer is the most widely used testing device for characterizing rheological properties of cementitious materials in the lab [43], but it should be noted that there are various types of rheometers. Previous studies observed meaningful

differences of a similar order between rheometers with different geometries and protocols [44]. In comparison of concrete mixtures, linear regression of the BTRHEOM τ_0 against the BML τ_0 yielded a slope of 1.66, and against the two-point τ_0 a slope of 1.225 [44]. These slopes indicate that τ_0 values obtained from the BTRHEOM were consistently higher than those from the BML and two-point rheometers for the same mixtures.

The regression slope is therefore interpreted throughout as an offset between measurement methods rather than a departure from a true value. The properties that determine practical usefulness are the precision of the correlation and the stability of that offset within a material class. Trueness is therefore evaluated in the ISO 5725-1 sense of closeness to an accepted reference value, here the vane rheometer τ_0 and not to a physical true value, which for a method-dependent quantity does not exist. A slope departing from unity accordingly denotes a stable inter-method offset relative to that accepted reference, not a measurement error.

The full and tip penetration can also be compared directly against each other. Their mutual regression (slope 1.05, 95% CI 0.94–1.16; intercept 1.02 kPa) is less precise than either configuration's agreement with the vane rheometer (R^2 = 0.78 versus 0.90). If the two configurations deviated from the reference identically, their mutual agreement would be at least as strong as their agreement with the vane rheometer; the lower value indicates instead that tip and full penetration deviate from the reference in different material classes, so that combining them compounds rather than cancels their respective errors. This provides the first indication that the reliability of each configuration depends on the testing material, a dependence examined in Section 3.2. Bland–Altman analysis confirms that the bias of both configurations is proportional rather than additive ($p < 0.001$), which is the property that makes such conversion feasible.

Repeatability: Probe-to-probe repeatability was quantified as the coefficient of variation among the three independent probe measurements taken at each mixture and age, expressed as a percentage of their mean; a lower value indicates closer agreement between probes. The probe repeatability was 7.9% for the tip and 7.4% for the full configuration; the residual scatter in Figure 4 therefore reflects genuine inter-method and inter-material variation rather than instrument noise. Another note to consider in this statistical analysis is that ordinary least squares regression treats the vane rheometer reference as error-free although it carries measurement scatter of its own, so the reported slopes are slightly attenuated and constitute conservative lower bounds on the true proportional bias. Furthermore, the pooled τ_0 range spans approximately two orders of magnitude (0.2–28 kPa), a span that in itself favors high pooled correlation; the more discriminating class-level evaluation follows in Section 3.2.

Overall, the combined dataset confirms that the test is applicable across the entire evaluated material space. Both penetration methods track the rheometer τ_0 with high precision; full penetration demonstrates high trueness, its proportional bias being near unity, whereas tip penetration exhibits a systematic yet correctable overestimation.

3.2 Evaluation of robustness across various material classes

The overall accuracy established in Section 3.1 does not guarantee uniform performance across all material classes; a method may agree with the reference on average while producing significant errors for specific materials. Figure 5 maps precision and trueness separately for each material class and penetration method. Cell color encodes precision (R^2), while the text annotations report trueness (regression slope) with its 95% CI and sample size. Classes with $n < 10$ are identified as indicative, since regression statistics at this sample size support direction-of-effect conclusions rather than quantitative conversion, whereas the larger classes ($n \geq 10$) are treated as quantitative.

Separating the two metrics reveals cases in which a strong correlation coexists with substantial systematic bias, reinforcing that high precision does not by itself imply trueness. The map is organized around the three material families evaluated in this study baseline mixtures, accelerated/structuring binders, and fiber-reinforced mixtures and addresses the questions motivating the work: whether measurement trueness is retained as binders are modified with SCMs, and whether it extends to fiber-reinforced systems.



Fig. 5 Test robustness map detailing the proportional bias (regression slope, the measure of trueness) and precision (R^2) of the tip and full penetration methods against the vane rheometer reference across material classes

Baseline binder systems: Across the baseline Type I binder systems (n = 30), full penetration reproduces the vane rheometer τ_0 without significant bias (slope 1.00, 95% CI 0.94–1.21) while tip penetration overestimates by roughly a factor of two (slope 1.98, 95% CI 1.77–2.44); both retain high precision (R^2 = 0.97 and 0.94, respectively). Within this family, the pozzolanic mixtures, incorporating fly ash and silica fume, track the reference closely for full penetration (slope 0.99, 95% CI 0.93–1.23; R^2 = 0.98, n = 24). This group also demonstrates the clearest example of high precision coexisting with systematic bias: for the silica-fume mixtures, tip penetration maintains a strong correlation with the rheometer (R^2 = 0.93, n = 18) while

overestimating the τ_0 twofold (slope 2.00, 95% CI 1.79–2.66). A printability threshold derived from an uncorrected tip measurement of these mixtures would therefore be inflated accordingly, confirming that a high coefficient of determination does not establish accuracy on its own.

The single inert-filler mixture, limestone in a Type I binder (n = 6), presents the complementary pattern. Full penetration remains near unity in slope (0.81, 95% CI 0.43–1.00) but at reduced precision relative to the pozzolanic mixtures ($R^2 = 0.91$), whereas tip penetration remains stable in both respects (slope 1.38, 95% CI 1.13–1.65; $R^2 = 0.98$). Because this observation rests on a single mixture and six measurements ($n < 10$), it is reported as an indicative reduction in precision requiring further confirmation rather than an established material effect. Taken across the baseline binders as a whole, the precision of full penetration remains well within the range required for practical τ_0 assessment.

Accelerated/structuring binder systems: A second binder family groups the Type III cement systems with some additives/admixtures to modify or accelerate early-age structural development: calcined clay, which affects thixotropy via particle agglomeration; VMA, which raises viscosity; and the higher hydration rate of the Type III cement itself. These constituents operate through different mechanisms but share the common functional role of promoting early-age structuration and are evaluated as a single family (n = 25). Full penetration overestimates the reference modestly across this family (slope 1.20, 95% CI 0.98–1.43; $R^2 = 0.92$). Within the family, the VMA-modified mixtures show the strongest agreement of any class evaluated, with near-unity slopes for both methods (full 1.02, 95% CI 0.65–1.17, $R^2 = 0.93$; tip 0.99, 95% CI 0.90–1.10, $R^2 = 0.98$; n = 10), consistent with the impact of VMA in suppressing flow-induced measurement scatter. The penetration tests in standard (non-VMA) mixtures overestimate more strongly for full penetration

(slope 1.27, 95% CI 1.04–1.59; $R^2 = 0.93$, n = 15). Both methods therefore remain applicable to this binder family, with the smallest bias observed in mixtures containing VMA.

Fiber-reinforced mixtures: Fiber reinforcement is where the tip and full penetration methods separate most clearly, and the separation is governed by fiber type. For the hemp mixtures (n = 18), both methods showed a good τ_0 measurement capability across the widest dosage range tested: full penetration is nearly unbiased (slope 1.03, 95% CI 0.81–1.19; $R^2 = 0.95$) and tip penetration overestimates by roughly half (slope 1.47, 95% CI 1.28–1.60) at high precision ($R^2 = 0.97$). For the steel fiber mixtures (n = 12), the two methods diverge in opposite directions: tip penetration doubles the reference value (slope 2.03, 95% CI 1.71–2.54) while preserving a strong correlation ($R^2 = 0.90$), whereas full penetration responds with reduced sensitivity, registering only 0.74 kPa per kPa of vane rheometer τ_0 (95% CI 0.54–0.98, excluding unity; $R^2 = 0.83$). The polypropylene mixtures (n = 12) show reduced precision for both methods (tip $R^2 = 0.68$; full $R^2 = 0.72$), with slope CIs too wide to support quantitative conversion (tip 1.38, 95% CI 0.88–1.85; full 0.83, 95% CI 0.49–1.12).

Classifying the fiber-reinforced mixtures by dosage isolates the conditions under which this reduced sensitivity arises. At high steel dosage, the full penetration slope falls to 0.61 (95% CI 0.22–0.99), while tip penetration retains high precision ($R^2 = 0.98$) alongside its consistent twofold overestimation (slope 2.02, 95% CI 1.64–2.40). At high polypropylene dosage, the full penetration slope CI encompasses zero (0.67, 95% CI −0.11–1.45), indicating that a statistically significant response to τ_0 cannot be established for this class. At low dosage, both fiber types perform consistently with their parent families. The hemp mixtures show high correlation at all dosages, with precision remaining high ($R^2 > 0.97$) for both methods and slopes ranging from 0.81 to 1.47. The reduced sensitivity of full penetration in closely spaced fiber mixtures is therefore governed

by dosage, emerging at high fiber content and affecting full penetration selectively while tip penetration continues to measure the τ_0 close to the reference measurement.

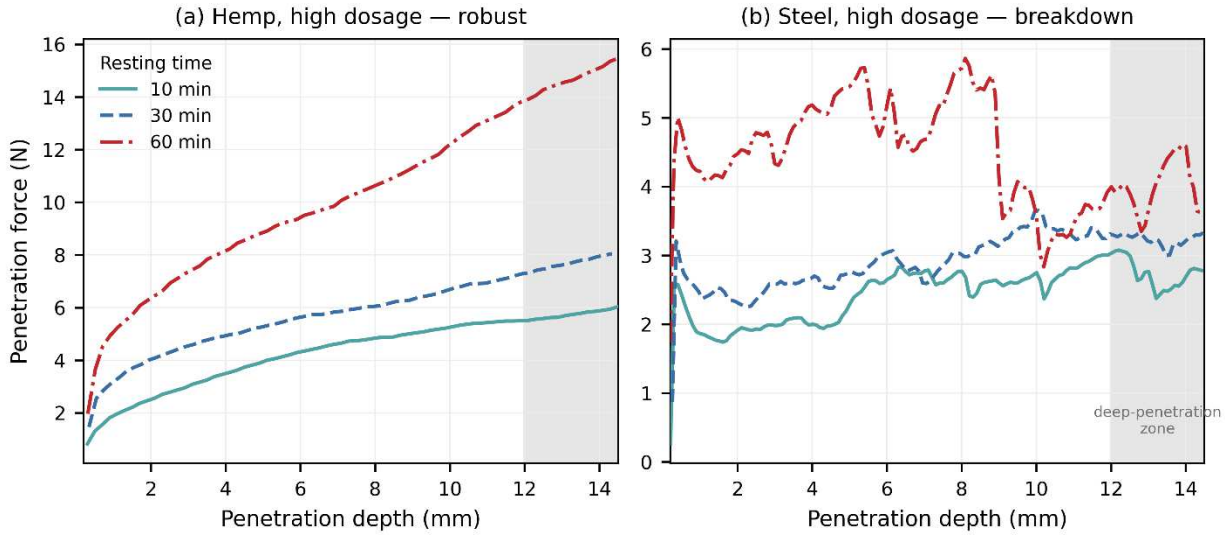

Fig. 6 Graphical representation of penetration force (N) versus penetration depth (mm) for high-dosage fiber-reinforced mixtures at different resting times (10, 30, and 60 min): (a) hemp fiber-reinforced mixture showing a robust, smooth response with penetration force increasing consistently with resting time; and (b) steel fiber-reinforced mixture exhibiting severe force fluctuations and signal breakdown due to fiber interference. The shaded region (12–15 mm) denotes the deep-penetration zone

To understand the underlying mechanisms in fiber-reinforced mixtures, Figure 6 displays the force-displacement diagrams for two contrasting cases. For the high-dosage hemp mixture, the full penetration record retains its characteristic shape and scales upward at different testing ages. For the high-dosage steel mixture, the full penetration record is irregular, and its deep-penetration plateau is nearly insensitive to age; the deep-zone force rises by 34% over the 10–60 min window, compared with 162% for hemp, thereby compressing the measured structuration into a narrow range, even as the peak force retains a weak age response.

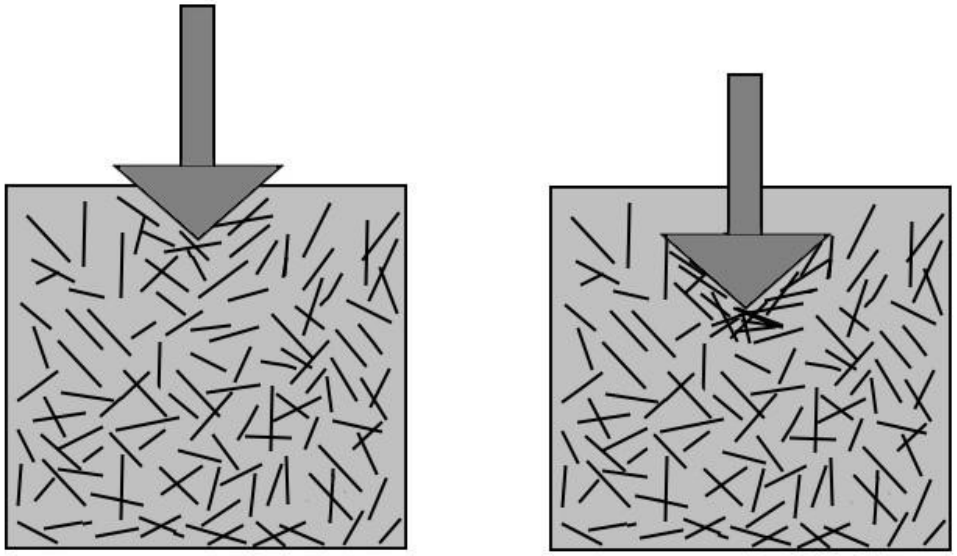

Fig. 7 Schematic illustration of fiber distribution during penetration testing: (a) tip penetration, representing the initial stage where the cone has entered the material but is not fully submerged, with minimal disturbance to the surrounding fibers; and (b) full penetration, where the cone is completely submerged, resulting in fiber reorientation, accumulation, and balling around the probe, leading to localized fiber concentration and increased probe–fiber interaction

A consistent mechanical interpretation follows from the relation between the probe's stressed zone and the density of the fiber network rather than from fiber stiffness alone. The fully submerged conical probe (20 mm base diameter, 10 mm height) mobilizes a failure zone tens of millimeters across, which is large relative to the mean inter-fiber spacing in the high-dosage mixtures. The spacing (s) is estimated as

$$s \approx d\sqrt{\frac{\pi}{4}V_f} \qquad \text{Eq. (2)}$$

where d is the diameter and V_f is the volume fraction of fibers. Eq. (2) gives 0.39 mm for the high-dosage polypropylene mixture, 1.45 mm for high-dosage steel, and 3.6 mm for high-dosage hemp; the corresponding fiber number densities differ by two orders of magnitude. Where spacing is small relative to the mobilized zone, the probe advances against a quasi-continuous fiber network whose resistance is largely independent of the matrix's structural build-up, so the measured force

decouples from the τ_0 the test is intended to capture. Figure 7 illustrates this: the advancing cone cannot pass between neighboring fibers and instead reorients and accumulates them ahead of and around itself. The shallow engagement of tip penetration stresses a smaller volume and preferentially samples matrix between fibers, so it continues to track build-up while local fiber interaction elevates the absolute reading. This ordering polypropylene most affected, then steel, then hemp follows inter-fiber spacing rather than fiber elastic modulus, which is consistent with a geometric network effect rather than a stiffness effect. The interpretation is offered as the reading most consistent with the present data; targeted experiments varying fiber number density at fixed probe geometry would be required to confirm it.

Each penetration method offers distinct advantages depending on the material: full penetration outperforms tip penetration in trueness for the silica fume mixtures, whereas tip penetration provides superior sensitivity in the closely spaced fiber networks of the high-dosage steel and polypropylene mixtures. The polypropylene mixtures remain the only class in which both methods perform comparably. Selecting the appropriate penetration method is therefore a material-dependent decision. Because the quantified systematic biases remain stable within their respective classes, they also present an opportunity for correction through class-specific conversion factors, developed in the next section.

3.3 Inter-method bias and conversion between methods

Sections 3.1 and 3.2 established that the two penetration methods deviate from the vane rheometer reference in stable, class-dependent ways. This section examines whether those deviations are systematic enough to be corrected, so that a measurement from one method can be converted to the quantity another method would report. The slump flow test is included not only as another fresh property measurement instrument but also because it is the most widely accepted indicator

of workability in practice and is often the quantity around which acceptance criteria are defined; a workability measurement device that can predict slump is therefore valuable independently of its agreement with the rheometer τ_0. The analysis below considers both conversion directions: converting between τ_0 methods and predicting slump from a τ_0 measurement.

Bias analysis: The tip penetration bias against the rheometer reference is not constant across materials. It ranges from near unity for the VMA-modified mixtures (slope 0.99, 95% CI 0.90–1.10) to approximately twofold for the silica fume and steel fiber mixtures (2.00 and 2.03, respectively). A single correction factor applied across all materials would therefore introduce errors of the same magnitude as the bias it aims to remove. Any usable conversion must instead be class specific. Before a correction can be proposed, the nature of the bias must be established: a bias that is a fixed offset, a bias that scales with magnitude, and a bias that is merely random scatter, each demands a different remedy, and only the first two are correctable at all. This distinction is assessed here using Bland–Altman analysis, which evaluates agreement between two methods by plotting the difference between paired readings against their mean, testing whether that difference is constant (additive bias) or grows with magnitude (proportional bias). The limits of agreement, expressed here in kPa (Full– rheometer: bias 0.43 kPa, 95% limits −4.18 to 5.05 kPa; Tip–rheometer: bias 1.75 kPa, 95% limits −4.61 to 8.11 kPa), widen visibly with increasing τ_0, consistent with proportional rather than fixed bias as shown in Figure 8. Because the bias is proportional, it is fully described by a single multiplicative factor per class, and the limits of agreement are reported here as multiplicative (×/÷) factors rather than as fixed ± intervals. Figure 9 presents the bias–scatter map, in which each material class appears as one point per method-pair, positioned by its proportional bias (regression slope) and its precision (R^2). This separates the

classes for which a reliable conversion exists from those for which the measurement is too scattered to convert.

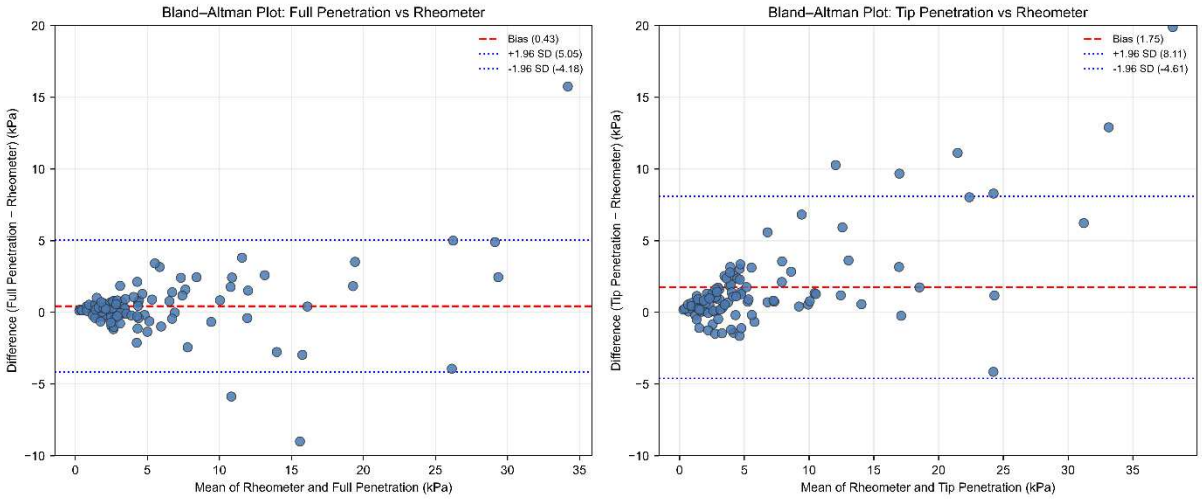

Fig. 8 Bland–Altman plot comparing the vane rheometer reference against: (a) full penetration; (b) tip penetration

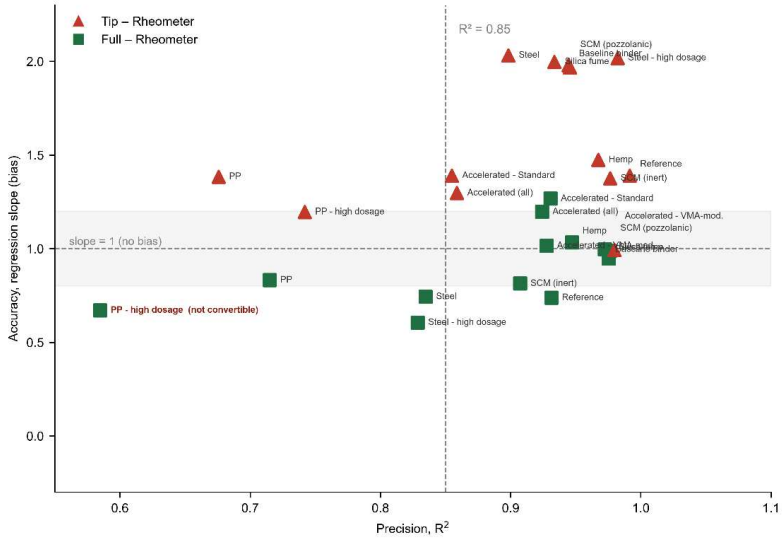

Fig. 9 Accuracy (regression slope) versus precision (R^2) for tip–rheometer and full–rheometer

Figure 9 separates the material classes into two groups. Classes in the upper-right region, with precision above $R^2 \approx 0.85$ and a slope CI that excludes zero, support a quantitative conversion factor; this covers the binder families and the hemp and steel fiber classes. Classes toward the lower-left, with reduced precision or a slope interval spanning zero cannot be corrected with

confidence; this includes the high-dosage polypropylene mixtures, where the full-penetration response to τ_0 is not statistically resolvable. The map therefore functions as a decision boundary, identifying at a glance which classes in Table 4 warrant a quantitative correction factor and which warrant only a qualitative direction-of-bias statement.

Conversion between penetration methods and the rheometer: Table 4 lists the class-specific factors with their CIs, sample sizes, and a confidence tier reflecting the discussion in Section 3.2. Full penetration requires little or no correction across most classes: its slope remains near unity for the baseline binders (1.00, 95% CI 0.94–1.21) and for the VMA-modified mixtures (1.02), rising modestly for the accelerated/structuring family (1.20). Tip penetration requires a larger but stable correction, close to a factor of two for the baseline binders (1.98) and the silica fume mixtures (2.00). One class is marked as non-convertible: the full-penetration reading of the high-dosage polypropylene mixtures, whose slope confidence interval encompasses zero. A further group is marked indicative rather than quantitative: the reference and inert-filler mixtures and all dosage-level classes, each resting on six mixture–age pairs, together with the polypropylene fiber class, whose precision (R^2 = 0.68 tip, 0.72 full) falls below the threshold for quantitative conversion.

Table 4 Class-specific conversion factors between tip/full penetration and rheometer τ_0, with 95% CIs and sample-size-based confidence tier

Material class	Method	n	Slope	95% CI		R^2	Confidence tier
			(conversion factor)	low	high		
Baseline Binder (all)	Tip	30	1.98	1.77	2.437	0.944	Q
	Full	30	0.996	0.94	1.213	0.972	Q
Reference (Type I, plain)	Tip	6	1.39	1.272	1.884	0.991	I
	Full	6	0.738	0.515	1.13	0.931	I
SCM (pozzolanic)	Tip	24	1.968	1.764	2.455	0.946	Q
	Full	24	0.988	0.931	1.227	0.976	Q
SCM (inert)	Tip	6	1.376	1.134	1.654	0.976	I
	Full	6	0.814	0.435	0.995	0.907	I
Accelerated/structuring (all)	Tip	25	1.297	0.898	1.636	0.859	Q

	Full	25	1.197	0.983	1.432	0.924	Q
	Tip	15	1.39	0.85	1.777	0.855	Q
Plain	Full	15	1.267	1.041	1.588	0.931	Q
	Tip	10	0.993	0.9	1.102	0.98	Q
VMA-modified	Full	10	1.015	0.645	1.169	0.928	Q
Fiber-reinforced (all)	Tip	42	1.293	1.008	1.418	0.914	Q
	Full	42	0.997	0.81	1.119	0.95	Q
	Tip	18	1.474	1.28	1.6	0.967	Q
Hemp	Full	18	1.034	0.814	1.19	0.947	Q
	Tip	12	1.384	0.881	1.855	0.676	I
PP	Full	12	0.832	0.491	1.119	0.715	I
	Tip	12	2.032	1.708	2.539	0.898	Q
Steel	Full	12	0.743	0.542	0.981	0.835	Q
PP, high dosage	Tip	6	1.196	0.217	2.175	0.742	I
	Full	6	0.67	-0.114	1.454	0.585	NC
Steel, high dosage	Tip	6	2.018	1.641	2.396	0.982	I
	Full	6	0.606	0.223	0.988	0.829	I

Q: Quantitative, I: Indicative (n<10), NC: Not Convertible

Predicting slump from a penetration reading: Slump is the property most commonly used for evaluating workability, therefore translating a rapid penetration reading directly into the slump value is at least as valuable as converting between τ_0 methods. The relationship between slump spread and τ_0 is nonlinear and was fitted in power-law form, with slump as the predicted quantity. Figure 10 presents these relationships for each material family. The predictive strength is strongly class dependent. For the baseline binder mixtures, full penetration predicts slump spread with high correlation ($R^2 = 0.90$), exceeding the rheometer itself ($R^2 = 0.84$); tip penetration performs comparably ($R^2 = 0.88$). For the accelerated/structuring mixtures, all three methods predict slump at a similar, moderate level ($R^2 = 0.67–0.81$). For the fiber-reinforced mixtures, predictive strength falls sharply: full penetration drops to $R^2 = 0.47$ and tip penetration to $R^2 = 0.24$, indicating that spread and τ_0 become decoupled once fibers are present that is, a given τ_0 no longer corresponds to a single, predictable spread value, because fiber content and geometry independently affect how the mixture flows. Combined across all mixtures, the rheometer predicts slump most strongly ($R^2 = 0.72$), followed by full penetration (0.60) and tip penetration (0.52).

The lack of correlation between penetration measurements and slump values in fiber-reinforced mixtures is consistent with the mechanism explained in Section 3.2. Fiber networks resist spreading through mechanical interlock that is largely independent of the matrix τ_0, so the slump spread of a fiber-reinforced mixture reflects fiber content and geometry in addition to τ_0, and no single τ_0 value maps uniquely to a spread. In the baseline and accelerated binder mixtures, where spread is governed by the matrix alone, a penetration measurement predicts slump as well as or better than the vane rheometer, which is a practically useful result given that penetration can be performed rapidly and repeatedly outside the laboratory. Slump is therefore best regarded as a fast-screening indicator that is reliably predictable from penetration for non-fiber mixtures, but that requires direct measurement once fibers are introduced. The class-specific conversion factors and their validity limits are consolidated into a practitioner-facing form in Section 3.5.

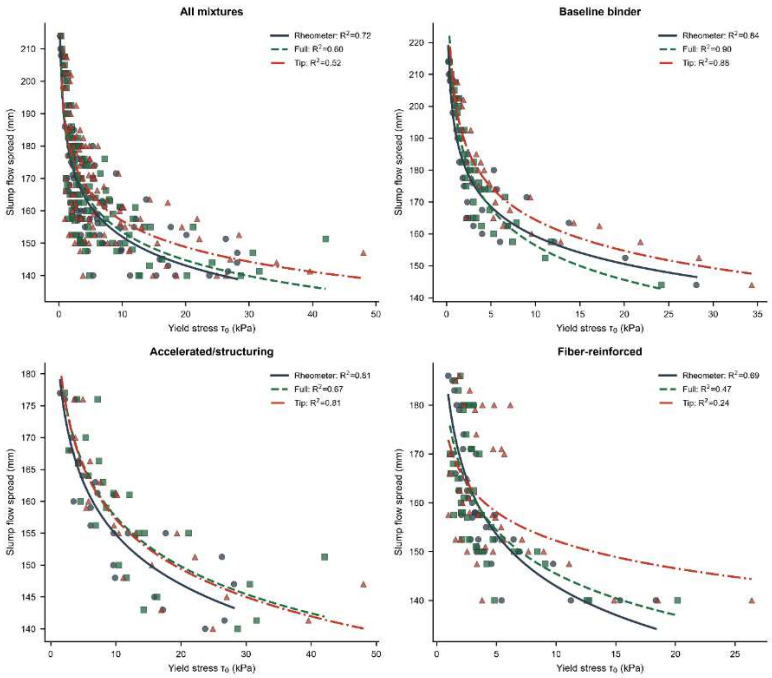

Fig. 10 Slump flow spread as a function of τ_0 for the rheometer, full penetration, and tip penetration methods, fitted as slump $= a \cdot {\tau_0}^b$ and faceted by material family

3.4 Structural build-up tracking

During the concrete printing process, each deposited layer must develop sufficient τ_0 to support subsequent layers, while the material must remain extrudable at the time of deposition. Buildability therefore depends not only on the τ_0 at any instant but on the rate at which it develops between depositions. This section evaluates whether the tip and full penetration methods reproduce the structural build-up rate obtained from the vane rheometer reference. The τ_0 development of all 18 mixtures follows an exponential trend over the evaluated 10- to 60-minute printing window and is modeled using Eq. (3):

$$\tau_0(t) = A \cdot e^{Bt} \quad \text{Eq. (3)}$$

where the exponent B (min^{-1}) is the structural build-up rate [45,46]. B is used as the tracking parameter in preference to a linear rate of τ_0 gain because a linear rate conflates the absolute magnitude of τ_0 with its rate of growth, whereas B expresses the relative growth rate independently of magnitude and is consistent with the observed exponential kinetics. Eq. (3) describes the data closely for all three methods ($R^2 \geq 0.80$ in all cases, above 0.93 for the large majority); Figure 11 illustrates the fit for a representative mixture. Across the 18 mixtures the rheometer-derived build-up rate B spans slow to fast structuring (roughly 0.016 to 0.097 min^{-1}), providing a wide dynamic range over which to test each method's performance.

Table 5 reports the fitted A and B parameters, fit quality, and the tracking error of each penetration method relative to the rheometer for all 18 mixtures; for reference, each mixture is classified as slow ($B < 0.03$ min^{-1}), moderate (0.03–0.04 min^{-1}), or fast structuring ($B > 0.04$ min^{-1}) by its rheometer -derived rate [13]. The analysis below is organized by the presence or absence of fibers, which the data identify as the primary factor governing tracking performance.

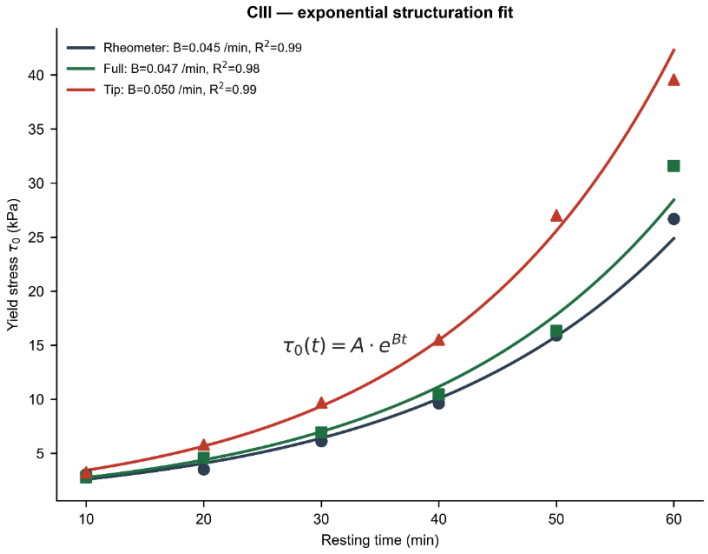

552

553 **Fig. 11** τ_0 development with resting time for the CIII mixture, with fitted exponential structuration curves
554 $\tau_0(t) = A \cdot e^{Bt}$ for all three methods

555 **Table 5** Exponential build-up rate (B), fit quality (R^2), and tracking error by mixture, method, and
556 structuration class

Mixture	Family	Class	Vane rheometer		Tip Penetration			Full Penetration		
			B (1/min)	R^2	B (1/min)	R^2	error (%)	B (1/min)	R^2	error (%)
Control	Binder-only	Moderate	0.031	0.955	0.034	0.975	10.2	0.021	0.977	30.3
30FA	Binder-only	Moderate	0.033	0.996	0.033	0.939	1.0	0.027	0.921	17.4
30FA_15SF	Binder-only	Moderate	0.034	0.986	0.031	0.958	7.7	0.027	0.988	19.7
5SF	Binder-only	Fast	0.043	0.969	0.049	0.971	12.0	0.038	0.982	11.4
10SF	Binder-only	Slow	0.022	0.935	0.031	0.83	45.9	0.023	0.972	4.9
15LF	Binder-only	Moderate	0.036	0.979	0.045	0.983	26.2	0.038	0.956	4.7
CIII	Binder-only	Fast	0.045	0.994	0.05	0.997	11.1	0.047	0.98	3.3
20CC	Binder-only	Moderate	0.038	0.958	0.046	0.931	19.4	0.041	0.991	6.2
20CC_15LF	Binder-only	Fast	0.097	1	0.075	1	22.2	0.088	0.972	8.8
20CC_VMA	Binder-only	Fast	0.041	0.993	0.04	0.963	3.3	0.036	0.98	13.5
30CC_15LF_VMA	Binder-only	Fast	0.046	0.99	0.05	0.975	7.7	0.038	0.93	16.8
ST_L	Fiber-reinforced	Slow	0.018	0.958	0.027	0.934	51.6	0.015	0.884	16.0
ST_H	Fiber-reinforced	Slow	0.021	0.955	0.022	0.983	3.7	0.01	0.867	51.2
PP_L	Fiber-reinforced	Slow	0.019	0.978	0.03	0.935	57.3	0.023	0.989	20.4
PP_H	Fiber-reinforced	Slow	0.016	0.805	0.025	0.942	54.9	0.016	0.828	0.8
HF_L	Fiber-reinforced	Moderate	0.039	0.974	0.044	0.981	11.8	0.04	0.966	0.1

HF_M	Fiber-reinforced	Slow	0.023	0.907	0.03	0.955	33.1	0.023	0.974	3.9
HF_H	Fiber-reinforced	Slow	0.018	0.971	0.027	0.968	44.8	0.024	0.955	32.0

For every mixture the rheometer-derived B serves as the reference (B_{ref}), and each penetration method is judged to track structuration faithfully when its build-up rate ($B_{test} = B_{tip}$ or B_{full}) matches B_{ref}. Agreement is quantified as the percentage deviation

$$\text{Percentage deviation} = \frac{|\,B_{test} - B_{ref}\,|}{B_{ref}} \times 100 \qquad \text{Eq. (4)}$$

This is a stricter test than correlation: two methods can both correlate strongly with resting time (high R^2) yet disagree on how fast τ_0 actually grows, and it is the growth rate, not the correlation, that governs how long a printed layer must wait before the next is placed.

Figure 12 compares the build-up rate derived from each penetration method against the build-up rate derived from the vane rheometer for all 18 mixtures, with ±10% and ±20% agreement bands. For the non-fiber mixtures (the baseline and accelerated/structuring families together), both methods reproduce the build-up rate measured by the rheometer with comparable trueness: the median deviation is 11% for both tip and full penetration, and the large majority of these mixtures fall within the ±20% band. Because the two readings are obtained from a single penetration operation, this close agreement means the result is robust regardless of which reading is used: the two provide a built-in consistency check and reports the build-up rate without loss of accuracy.

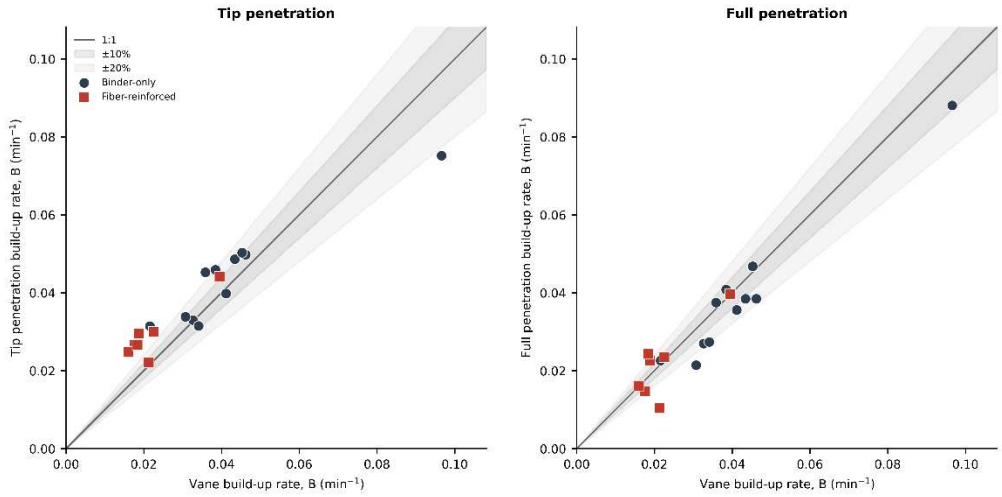

Fig. 12 Penetration-derived structural build-up rate (B) versus the rheometer -derived rate for all 18 mixtures, with ±10%/±20% agreement bands. Fiber-reinforced mixtures are marked separately

The fiber-reinforced mixtures distinguish the two methods sharply, and in the direction opposite to the point-measurement results of Section 3.2. Tip penetration overstates the build-up rate in all seven fiber-reinforced mixtures, with a median deviation of 45%, whereas full penetration reproduces the vane rheometer rate with a median deviation of 16% and remains within 20% for most fiber classes. Because the fiber-reinforced mixtures cluster at the low end of the build-up range ($B_{ref} \approx 0.016–0.023$ min^{-1}), a fixed absolute error maps onto a large percentage deviation, so these magnitudes are amplified relative to those of the faster-structuring binder mixtures; the isolated 32% full-penetration deviation for the high-dosage hemp mixture arises the same way, from a small absolute error on a low B_{ref}. The direction of the effect is not an artifact, however: full penetration reproduces these same low-B vane rheometer rates with a median deviation of 16% on the identical mixtures, so the tip-specific overshoot reflects a genuine measurement bias rather than denominator sensitivity alone. The single exception is the high-dosage steel mixture, for which full penetration deviates by 51%. This is the same class in which Section 3.2 identified a loss of sensitivity of the full penetration method and therefore represents an expected boundary rather than a new one. A consistent interpretation follows from the mechanism proposed there: the

shallow tip engagement samples the matrix together with local fiber interaction, and as the fiber network consolidates with resting time this interaction adds an apparent structuration on top of the true matrix build-up, inflating build-up rate B. The deep zone mobilized by full penetration averages over the network and follows the matrix trend, except where a dense stiff-fiber network dominates the response entirely.

These results refine the guidance for method selection. For measuring instantaneous τ_0 in fiber-reinforced mixtures, Section 3.2 identified tip penetration as the configuration that retained sensitivity with a stable, correctable bias, whereas full penetration lost sensitivity; for the build-up rate of the same mixtures, full penetration is the more faithful method, provided stiff-fiber dosage remains below the sensitivity boundary. The two findings are complementary rather than contradictory: the appropriate penetration configuration depends not only on the material class but on the quantity of interest, the current τ_0 or its rate of development. In short, the configuration best suited to reading τ_0 magnitude is not the one best suited to reading its rate of change. For non-fiber mixtures both configurations track the build-up rate within practical tolerance, and a printing schedule based on penetration-derived B would incur rate errors comparable to the repeatability of the vane rheometer reference itself. Consolidated selection guidance combining both criteria is presented in Section 3.5.

3.5 Method selection

Sections 3.1 through 3.4 evaluated tip and full penetration against four separate criteria: overall correlation of penetration measurements against the vane rheometer as a reference, trueness and precision within individual material classes, translatability through class-specific conversion factors, and faithfulness in tracking the structural build-up rate. Taken individually, no one criterion determines which method is superior. This section consolidates the four into a single selection

framework. The organizing result is that the preferred penetration method is governed jointly by two factors: the material class, and the quantity of interest i.e. the instantaneous τ_0 at a given moment, or the build-up rate B at which the structuration develops. Because the tip and full penetration readings are obtained one after another as outlined in Section 2.3.1, the practical question is not which test to run but which of the two readings to report for a given quantity. The guidance below is framed accordingly.

Table 6 summarizes the resulting guidance. Each row of Table 6 reports, for one material class, the preferred method for measuring τ_0 magnitude together with its conversion factor relative to the rheometer, the preferred method for tracking the build-up rate B, whether slump is predictable from a penetration reading, and the principal validity limit. The conversion factors are multiplicative and class-specific: a factor of 1.0 indicates that the method reproduces the rheometer τ_0 without correction, while a factor of 2.0 indicates a twofold proportional bias that a single multiplication removes. Factors derived from classes of ten or more mixture–age pairs are treated as quantitative; those derived from the six-pair dosage-level classes are reported as indicative, supporting the direction of the correction rather than its precise value. Where a class is marked "not recommended," the response of that method to τ_0 could not be quantified for the class, its slope CI encompasses zero, and the entry denotes an absence of a usable relationship rather than a material deficiency; in every such case the complementary method remains valid and is the one listed.

Table 6 Recommended penetration method by material class and quantity of interest, with rheometer conversion factors and validity limits

Material class	τ_0 (conversion factor)	Build-up rate	Slump predictable from penetration	Principal validity limit
Baseline binder (Type I; fly ash, silica fume)	Full (×1.0) or tip (×2.0); both high precision	Either (median deviation 11%)	Yes, full predicts slump as well as or better than the rheometer	Inert-filler (limestone) rests on n = 6; indicative only
Accelerated / structuring (Type III; calcined clay, VMA)	Full (×1.2); VMA subclass ×1.0 for both methods	Either (within practical tolerance)	Moderate (all three methods comparable)	—
Fiber: hemp (flexible), all dosages	Full (×1.0) or tip (×1.5); both valid at every dosage tested	Full preferred (median deviation 16%)	No, measure slump directly	Robustness established within the tested hemp formulations
Fiber: steel (rigid)	Tip (×2.0, stable); full loses sensitivity at high dosage	Full preferred, except at high dosage	No, measure slump directly	High dosage is the sensitivity boundary; n = 6, indicative
Fiber: polypropylene	Tip preferred; full not recommended at high dosage	Full preferred (tip overstates)	No, measure slump directly	Reduced precision for both methods; full not quantifiable at high dosage

For the non-fiber families, the selection is unambiguous. Full penetration reproduces the vane rheometer τ_0 with little or no correction across the baseline and accelerated/structuring binders, while tip penetration requires a stable class-specific correction factor, close to twofold for the baseline and silica-fume mixtures, and near unity where a VMA is present. For the rate of development, both methods reproduce the rheometer-derived build-up rate B to within a median deviation of 11% for these materials. Because both are generated by the same penetration operation, this alignment demonstrates the result is independent of the selected reading. Consequently, the two methods offer an internal validation check, and either can determine the build-up rate without a loss of accuracy.

Slump is also predictable from a penetration reading for these mixtures, within the baseline family as well as or better than from the vane rheometer itself, which makes penetration a practical single instrument for both τ_0 and workability screening. Across these families the precision of both methods remains well within the range required for practical τ_0 assessment.

The fiber-reinforced family requires the method to be matched to the quantity of interest, and this is where the full penetration and tip penetration methods separate most clearly. For hemp, a flexible natural fiber, both methods measure τ_0 magnitude accurately at every dosage tested, and full penetration is the more faithful tracker of the build-up rate. For the rigid fibers, steel and polypropylene, the two quantities call for different methods: tip penetration is preferred for τ_0 magnitude, retaining sensitivity to τ_0 with a stable, correctable bias, whereas full penetration is preferred for the build-up rate. The exception is the high-dosage stiff-fiber boundary, at which the deep zone mobilized by full penetration engages a load-bearing fiber network and its response to τ_0 magnitude can no longer be quantified; tip penetration continues to measure magnitude at this boundary, and full penetration continues to track the rate for all but the densest stiff-fiber network. Slump becomes decoupled from τ_0 once fibers are present and must be measured directly rather than inferred from a penetration reading. The practical consequence is the central selection rule of this study: for fiber-reinforced mortars, the reading best suited to τ_0 magnitude is not the one best suited to evaluate its rate of change. Because a single penetration operation delivers both, this is a practical advantage rather than a limitation: from one test on a fiber-reinforced mortar, the tip reading supplies the magnitude-appropriate estimate and the full reading the rate-appropriate one, with no separate measurement or change of instrument required to obtain either. The systematic divergence between the two penetration modes for stiff-fiber mortars, which is largely absent in unreinforced mixtures, likely indicates the development of a load-bearing fiber network.

Establishing this divergence as a quantitative diagnostic metric remains a key research objective for future work.

The specification of τ_0 limits requires the same consideration. τ_0 has no single absolute value: even the τ_0 obtained from the reference vane rheometer is one operational measurement, with comparable differences reported between rheometer types used in the same material [43,44]. The systematic offsets quantified in Sections 3.2 and 3.3 are of the same character: stable, class-specific, and of an order consistent with documented inter-instrument variability, and are addressed by calibration through the conversion factors of Table 6 rather than treated as measurement error to be removed. This interpretation applies to the classes in which the penetration reading retains a well-defined, precise response to τ_0; it does not extend to the high-dosage stiff-fiber classes in which the full-penetration response to τ_0 could not be resolved, which represent a genuine limit of that reading rather than an offset. On this basis, any printability threshold or structuration target is a method-indexed quantity: a limit established with one method is not interchangeable with the same numerical value measured by another without the applicable class-specific factor. A threshold derived from an uncorrected tip measurement of a silica-fume mixture, for example, would be inflated approximately twofold relative to the rheometer value. Acceptance criteria and printability windows should therefore state the method and the class-specific factor on which they are based, so that a limit measured in the laboratory can be reproduced on site with the method available there.

These recommendations are established under defined conditions. All specimens were mold-cast and tested under laboratory conditions; evaluation on deposited filaments during printing was not investigated and is the necessary next step. All penetration measurements were made at a single probe speed of 1 mm/s, and the conversion factors reported here apply to that speed. The inert-

filler and dosage-level classes rest on six mixture–age pairs each and are reported as indicative, supporting the direction of an effect rather than a quantitative factor. The hemp mixtures were formulated with matrix and admixture adjustments that differ from the other fiber mixtures, so their robustness is claimed within the tested formulations. Finally, the ordinary-least-squares regressions treat the vane rheometer reference as error-free although it carries measurement scatter of its own; the reported slopes are consequently slightly attenuated and constitute conservative lower bounds on the true proportional bias. Evaluation of the same methods directly on printed filaments, across a range of penetration speeds, is identified as the priority for extending this framework to in-line process control.

4. Conclusion

This study evaluated tip and full penetration as practical methods for measuring static yield stress (τ_0) and its rate of development in 3DCP mortars, across 18 mixtures spanning two cement types, four SCMs, and three fiber types, benchmarked simultaneously against the vane rheometer and the mini slump on the same batches. The following conclusions are drawn from this evaluation.

- Both methods tracked the rheometer-derived τ_0 across the full matrix with high precision ($R^2 = 0.90$ for both, $n = 103$) but diverged sharply in trueness: full penetration reproduced the rheometer value with a near-unity slope (1.07, 95% CI 1.001–1.144), while tip penetration overestimated it systematically by 27% (slope 1.27, 95% CI 1.19–1.36). High precision did not guarantee accuracy. Tip penetration on silica-fume mixtures, for example, retained a strong correlation ($R^2 = 0.93$) while overestimating τ_0 twofold (slope 2.00). Therefore, correlation strength alone is an insufficient criterion for validating a penetration method; the regression slope must be reported and evaluated independently of R^2.

- Method performance was not uniform across material classes. Full penetration required little or no correction for most binder and fiber classes, but its response to τ_0 became statistically unresolvable at high fiber dosages (steel: slope 0.61, 95% CI 0.22–0.99; polypropylene: slope 0.67, 95% CI −0.11–1.45, encompassing zero). Tip penetration remained sensitive to τ_0 at these same dosages, retaining a stable, correctable twofold bias. The two methods are therefore complementary rather than interchangeable, and selection must be matched to material class.

- The bias between methods was proportional rather than additive (Bland–Altman, $p < 0.001$) and stable within material classes, enabling correction through class-specific conversion factors ranging from near unity (0.99, VMA-modified mixtures) to approximately twofold (2.00–2.03, silica fume and steel-fiber mixtures). A single pooled factor is not appropriate given this range; correction must be applied at the class level, and dosage-level factors ($n = 6$) are indicative rather than quantitative.

- Penetration readings predicted slump flow as reliably as the vane rheometer itself in non-fiber mixtures (full penetration $R^2 = 0.90$ for baseline binders, exceeding the vane's own $R^2 = 0.84$), making penetration a practical single instrument for both τ_0 and workability screening in these mixtures. This predictive relationship broke down once fibers were present (R^2 falling to 0.47 for full and 0.24 for tip), because fiber networks affect spread independently of τ_0; slump should therefore be measured directly, not inferred, in fiber-reinforced mixtures.

- Both methods tracked the structural build-up rate B within a median deviation of 11% of the rheometer-derived rate for non-fiber mixtures, so either method can be used interchangeably for this purpose. In fiber-reinforced mixtures the two methods diverged in

the direction opposite to their τ_0 performance: tip penetration overstated the build-up rate (median deviation 45%), while full penetration remained faithful to the vane rheometer rate (median deviation 16%, exceeding 20% only at the same high-stiff-fiber dosage identified as the full-penetration sensitivity boundary above). The method best suited to reading τ_0 magnitude in fiber-reinforced mortars is therefore not the one best suited to reading its rate of change. Tip penetration is best for magnitude, while full penetration is best for rate. Because both readings are obtained from a single penetration operation; both quantities are available from one test.

- Probe-to-probe repeatability was 7.9% (tip) and 7.4% (full) across the full matrix, including the fiber-reinforced mixtures, confirming that fiber reinforcement does not degrade the reproducibility of either method.

- These findings support the practitioner selection framework of Table 6: full penetration for non-fiber and hemp mixtures across both τ_0 magnitude and build-up rate; for rigid-fiber mixtures, tip penetration for magnitude and full penetration for rate, until the high-dosage sensitivity boundary is reached, beyond which tip penetration alone remains valid for magnitude.

- These conclusions rest on mold-cast specimens tested at a single probe speed (1 mm/s), against a vane reference that is itself one operational realization of τ_0 among several established rheometer geometries. Evaluation of both penetration methods directly on deposited filaments during printing, and across a range of probe speeds, is identified as the necessary next step toward in-line process control.

Statements and Declarations

Availability of data and material: All data generated or analyzed during this study are included in this published article (Appendix, Tables App. 1a–1b). Raw force–displacement records are available from the corresponding author on reasonable request.

Competing Interests: The authors declare a pending US patent on one of the devices used in this study. This patent is relevant to the research presented in this manuscript. No financial benefits or royalties have been received to date, and the authors declare there are no other conflicts of interest.

Funding resources: This research did not receive any specific grant from funding agencies in the public, commercial, or non-profit sectors. The authors would like to thank Center for Infrastructure Engineering Studies for their support in conducting the experiments.

Author contributions:

Shiva Kumar Goud Kasani: Writing – original draft, Visualization, Validation, Conceptualization

Ali Fasihi: Writing – review & editing, Methodology, Conceptualization.

Nicolas A. Libre: Writing – review & editing, Supervision, Software, Project administration, Methodology, Investigation, Conceptualization.

References

1. Buswell RA, De Silva WL, Jones SZ, Dirrenberger J (2018) 3D printing using concrete extrusion: A roadmap for research. Cem Concr Res 112:37–49. https://doi.org/10.1016/j.cemconres.2018.05.006

2. Bradford K, Gentry R, Ben-Alon L, Kurtis K (2025) Construction 3D printing material selection: Minimizing cost and carbon footprint of residential wall assemblies. Constr Build Mater 493:143150. https://doi.org/10.1016/j.conbuildmat.2025.143150

3. Nodehi M, Ozbakkaloglu T, Gholampour A (2022) Effect of supplementary cementitious materials on properties of 3D printed conventional and alkali-activated concrete: A review. Autom Constr 138:104215. https://doi.org/10.1016/j.autcon.2022.104215

4. Kasani SKG, Fasihi A, Libre NA (2026) Exploring SCMs and fibers for structural build-up in 3D printing using penetration test. In: Miners Solving for Tomorrow Research Conference, Missouri University of Science and Technology, Rolla, Missouri

5. Xia Z, Geng J, Zhou Z, Liu G (2025) Comparative analysis of polypropylene, basalt, and steel fibers in 3D printed concrete: Effects on flowability, printability, rheology, and mechanical performance. Constr Build Mater 465:140098. https://doi.org/10.1016/j.conbuildmat.2025.140098

6. Sadrmomtazi A, Fasihi A (2010) Preliminary study on the mechanical behavior of mortar containing waste polypropylene fiber and nano-SiO_2. In: Proceedings of the 2nd International Conference on Sustainable Construction Materials and Technologies, vol 1, pp 209–216

7. Ngo TH, Li S, Huynh T, Zhang YX, Tran P (2025) 3D printable hemp concrete: Rheological, mechanical, and microstructural properties. J Build Eng 114:114467. https://doi.org/10.1016/j.jobe.2025.114467

8. Chen Z, Zhao G, Chen B, Chen S, Li J, Nong Y (2024) Influence of flocculation structure on time-dependent fluidity and rheological property of cement paste: Analytical models based on fractal theory. Constr Build Mater 455:139137. https://doi.org/10.1016/j.conbuildmat.2024.139137

9. Zhao X, Wang H, Luo G, Dai K, Hu Q, Jin J et al (2024) Study on the rheological and thixotropic properties of fiber-reinforced cemented paste backfill containing blast furnace slag. Minerals 14:964. https://doi.org/10.3390/min14100964

10. Sharma A, Gupta S, Noman Husain M, Chaudhary S (2025) Factors affecting the rheology of cement-based composites: A review. J Am Ceram Soc 108:e20429. https://doi.org/10.1111/jace.20429

11. Martinie L, Rossi P, Roussel N (2010) Rheology of fiber reinforced cementitious materials: classification and prediction. Cem Concr Res 40:226–234. https://doi.org/10.1016/j.cemconres.2009.08.032

12. Le TT, Austin SA, Lim S, Buswell RA, Gibb AG, Thorpe T (2012) Mix design and fresh properties for high-performance printing concrete. Mater Struct 45:1221–1232. https://doi.org/10.1617/s11527-012-9828-z

13. Perrot A, Rangeard D, Pierre A (2016) Structural built-up of cement-based materials used for 3D-printing extrusion techniques. Mater Struct 49:1213–1220. https://doi.org/10.1617/s11527-015-0571-0

14. Roussel N (2018) Rheological requirements for printable concretes. Cem Concr Res 112:76–85. https://doi.org/10.1016/j.cemconres.2018.04.005

15. Vallurupalli K, Libre NA, Khayat KH (2024) Characterization of extrudability using rheology and desorptivity. ACI Mater J 121:5–15. https://doi.org/10.14359/51740301

16. Harbouz I, Yahia A, Roziere E, Loukili A (2023) Printing quality control of cement-based materials under flow and rest conditions. Cem Concr Compos 138:104965. https://doi.org/10.1016/j.cemconcomp.2023.104965

17. Gu YC, Khayat KH (2024) Extrudability window and offline test methods to predict buildability of 3D printing concrete. Cem Concr Res 182:107552. https://doi.org/10.1016/j.cemconres.2024.107552

18. Estelle P, Lanos C (2012) High torque vane rheometer for concrete: principle and validation from rheological measurements. Appl Rheol 22:12881. https://doi.org/10.3933/applrheol-22-12881

19. Jacquet Y, Perrot A (2023) Sewing concrete device—combining in-line rheology control and reinforcement system for 3D concrete printing. Materials 16:5110. https://doi.org/10.3390/ma16145110

20. de la Flor Juncal L, Scott A, Clucas D, Loporcaro G (2025) Ultrasonic pulse velocity for real-time filament quality monitoring in 3D concrete printing construction. Buildings 15:2566. https://doi.org/10.3390/buildings15142566

21. Lootens D, Jousset P, Martinie L, Roussel N, Flatt RJ (2009) Yield stress during setting of cement pastes from penetration tests. Cem Concr Res 39:401–408. https://doi.org/10.1016/j.cemconres.2009.01.012

22. Sleiman H, Perrot A, Amziane S (2010) A new look at the measurement of cementitious paste setting by Vicat test. Cem Concr Res 40:681–686. https://doi.org/10.1016/j.cemconres.2009.12.001

23. Pott U, Stephan D (2021) Penetration test as a fast method to determine yield stress and structural build-up for 3D printing of cementitious materials. Cem Concr Compos 121:104066. https://doi.org/10.1016/j.cemconcomp.2021.104066

24. Reiter L, Wangler T, Roussel N, Flatt RJ (2022) Slow penetration for characterizing concrete for digital fabrication. Cem Concr Res 157:106802. https://doi.org/10.1016/j.cemconres.2022.106802

25. Lu H, Zhang L, Wang J, Shi Z, She W, Zuo W (2025) Penetration test of sheet-like indenter for yield stress assessment of 3D-printed concrete. Cem Concr Res 188:107728. https://doi.org/10.1016/j.cemconres.2024.107728

26. Barry M, Jacquet Y, Perrot A (2025) Pocket vane and penetrometer as quality control tool for extrusion 3D concrete printing. Mater Struct 58:297. https://doi.org/10.1617/s11527-025-02831-6

27. Boujlel J, Coussot P (2012) Measuring yield stress: a new, practical, and precise technique derived from detailed penetrometry analysis. Rheol Acta 51:867–882. https://doi.org/10.1007/s00397-012-0643-9

28. Rehman AU, Kim IG, Kim JH (2024) Towards full automation in 3D concrete printing construction: Development of an automated and inline sensor-printer integrated instrument for in-situ assessment of structural build-up and quality of concrete. Dev Built Environ 17:100344. https://doi.org/10.1016/j.dibe.2024.100344

29. Fasihi A, Libre NA (2025) Towards accurate in-situ static yield stress measurement for 3D concrete printing: A study on novel fast penetration test. J Build Eng 108:113002. https://doi.org/10.1016/j.jobe.2025.113002

30. Fasihi A, Libre NA (2026) Tip penetration test for rapid in-line assessment of static yield stress during 3D concrete printing process. Cem Concr Compos 166:106412. https://doi.org/10.1016/j.cemconcomp.2025.106412

31. Mazhoud B, Perrot A, Picandet V, Rangeard D, Courteille E (2019) Underwater 3D printing of cement-based mortar. Constr Build Mater 214:458–467. https://doi.org/10.1016/j.conbuildmat.2019.04.134

32. Khayat KH, Omran AF, Naji S, Billberg P, Yahia A (2012) Field-oriented test methods to evaluate structural build-up at rest of flowable mortar and concrete. Mater Struct 45:1547–1564. https://doi.org/10.1617/s11527-012-9856-8

33. ASTM C150/C150M-22 (2022) Standard specification for Portland cement. ASTM International, West Conshohocken, PA

34. ASTM C618-25 (2025) Standard specification for coal ash and raw or calcined natural pozzolan for use in concrete. ASTM International, West Conshohocken, PA

35. da Costa Santos AC, Archbold P (2022) Suitability of surface-treated flax and hemp fibers for concrete reinforcement. Fibers 10:101. https://doi.org/10.3390/fib10110101

36. Sedan D, Pagnoux C, Smith A, Chotard T (2008) Mechanical properties of hemp fibre reinforced cement: Influence of the fibre/matrix interaction. J Eur Ceram Soc 28:183–192. https://doi.org/10.1016/j.jeurceramsoc.2007.05.019

37. Baldwin Z, Fasihi A, Libre NA (2024) Feasibility of using hemp fiber reinforcement in 3D printing cementitious composites. In: 19th Annual Undergraduate Research Conference (UGRC), 2024, Missouri University of Science and Technology, Rolla, Missouri

38. Rahman M, Rawat S, Yang RC, Mahil A, Zhang YX (2024) A comprehensive review on fresh and rheological properties of 3D printable cementitious composites. J Build Eng 91:109719. https://doi.org/10.1016/j.jobe.2024.109719

39. Li H, Wei J, Khayat KH (2024) 3D printing of fiber-reinforced calcined clay-limestone-based cementitious materials: From mixture design to printability evaluation. Buildings 14:1666. https://doi.org/10.3390/buildings14061666

40. ASTM C1437-20 (2020) Standard test method for flow of hydraulic cement mortar. ASTM International, West Conshohocken, PA

41. Fasihi A, Libre NA (2024) From pumping to deposition: A comprehensive review of test methods for characterizing concrete printability. Constr Build Mater 414:134968. https://doi.org/10.1016/j.conbuildmat.2024.134968

42. Libre NA, Khoshnazar R, Shekarchi M (2012) Repeatability, responsiveness and relative cost analysis of SCC workability test methods. Mater Struct 45:1087–1100. https://doi.org/10.1617/s11527-011-9818-6

43. Roussel N, Bessaies-Bey H, Kawashima S, Marchon D, Vasilic K, Wolfs R (2019) Recent advances on yield stress and elasticity of fresh cement-based materials. Cem Concr Res 124:105798. https://doi.org/10.1016/j.cemconres.2019.105798

44. Beaupré D, Chapdelaine F, Domone P, Koehler E, Shen L, Sonebi M et al (2004) Comparison of concrete rheometers: International tests at MBT (Cleveland OH, USA) in May 2003. NISTIR 7154. National Institute of Standards and Technology, Gaithersburg, MD. https://doi.org/10.6028/NIST.IR.7154

45. Roussel N (2006) A thixotropy model for fresh fluid concretes: theory, validation and applications. Cem Concr Res 36:1797–1806. https://doi.org/10.1016/j.cemconres.2006.05.025

46. Perrot A, Pierre A, Vitaloni S, Picandet V (2015) Prediction of lateral form pressure exerted by concrete at low casting rates. Mater Struct 48:2315–2322. https://doi.org/10.1617/s11527-014-0313-8

Appendix:

The experimental results for vane rheometer, mini slump, tip and full penetration tests for baseline mixtures, accelerated/structured binders and fiber-reinforced mixtures at penetration speed of 1mm/s tabulated in Table App.1a – 1b.

Table App. 1a Summarized results for baseline mixtures

No	Mix Code	Vane rheometer τ0 (kPa)	Tip penetration τ0 (kPa)	Full Penetration τ0 (kPa)	Mini slump (mm)
1	Control	0.64	0.70	0.88	205
2	Control	0.76	1.03	1.06	202.5
3	Control	0.98	1.44	1.44	202.5
4	Control	1.25	1.84	1.48	190
5	Control	2.39	3.35	2.04	185
6	Control	2.63	3.54	2.65	180
7	30FA	0.20	0.39	0.33	214
8	30FA	0.28	0.54	0.49	210
9	30FA	0.38	0.93	0.52	208
10	30FA	0.58	1.22	0.98	207.5
11	30FA	0.75	1.90	0.86	202
12	30FA	1.00	1.74	1.40	200
13	30FA_15SF	0.69	1.14	1.22	198
14	30FA_15SF	1.13	1.83	1.63	192.5
15	30FA_15SF	1.66	2.73	1.95	192.5

16	30FA_15SF	2.26	3.85	3.05	182.5
17	30FA_15SF	2.91	4.79	3.63	176
18	30FA_15SF	4.00	5.39	4.70	174
19	5SF	1.44	2.28	1.78	182.5
20	5SF	1.82	2.79	2.11	177.5
21	5SF	2.33	5.49	3.02	170
22	5SF	4.00	7.12	4.83	167.5
23	5SF	6.91	17.19	6.90	162.5
24	5SF	12.13	21.81	11.73	157.5
25	10SF	1.97	3.59	2.22	175
26	10SF	2.22	2.18	3.00	165
27	10SF	2.49	5.28	3.32	165
28	10SF	3.01	6.35	3.93	162.5
29	10SF	4.00	9.58	5.29	160
30	10SF	6.02	12.85	7.42	157.5
31	15LF	5.32	4.22	3.20	180
32	15LF	5.67	5.50	4.32	174
33	15LF	9.01	9.41	6.57	171.5
34	15LF	13.76	14.32	7.89	163.5
35	15LF	20.10	28.39	11.09	152.5
36	15LF	28.11	34.33	24.18	144

Table App.1b Summarized results accelerated/structured binders and fiber-reinforced mixtures

No	Mix Code	Vane rheometer τ0 (kPa)	Tip penetration τ0 (kPa)	Full Penetration τ0 (kPa)	Mini slump (mm)
1	CIII	3.04	3.24	2.78	168
2	CIII	3.50	5.79	4.58	160
3	CIII	6.13	9.70	6.92	156.2
4	CIII	9.61	15.54	10.44	150
5	CIII	15.90	27.02	16.31	145
6	CIII	26.68	39.60	31.58	141.3
7	20CC	4.42	4.23	4.16	166
8	20CC	4.88	5.78	5.77	164
9	20CC	6.84	7.66	8.02	163
10	20CC	9.65	10.19	12.08	161
11	20CC	17.65	19.39	21.17	155
12	20CC	28.13	48.03	30.59	147
13	20CC_15LF	3.81	4.93	7.23	176
14	20CC_15LF	9.66	10.44	13.48	155
15	20CC_15LF	26.30	22.16	42.07	151.3
16	20CC_15LF	-	-	-	-

17	20CC_15LF	-	-	-	-
18	20CC_15LF	-	-	-	-
19	20CC_VMA	1.44	1.64	2.16	177
20	20CC_VMA	2.18	3.61	4.04	176
21	20CC_VMA	3.23	3.76	5.36	170
22	20CC_VMA	4.27	6.04	7.43	166.3
23	20CC_VMA	7.19	10.03	9.64	161.3
24	20CC_VMA	11.85	13.04	14.44	155
25	30CC_15LF_VMA	6.12	5.45	8.53	159
26	30CC_15LF_VMA	9.89	11.17	11.67	148
27	30CC_15LF_VMA	17.23	16.99	14.27	143
28	30CC_15LF_VMA	23.72	24.90	28.73	140
29	30CC_15LF_VMA	-	-	-	-
30	30CC_15LF_VMA	-	-	-	-
31	ST_L	1.32	1.57	1.51	185
32	ST_L	1.67	2.30	2.30	180
33	ST_L	2.24	3.31	2.48	174
34	ST_L	2.20	4.73	2.90	171
35	ST_L	2.85	5.42	2.92	171
36	ST_L	3.29	5.66	3.57	170
37	ST_H	0.97	1.89	1.98	186
38	ST_H	1.47	2.77	1.82	183
39	ST_H	1.88	3.20	2.24	179
40	ST_H	2.09	3.82	2.77	180
41	ST_H	2.43	4.80	2.73	180
42	ST_H	3.12	6.16	3.08	180
43	PP_L	1.31	1.11	1.11	170
44	PP_L	1.71	1.76	1.36	168
45	PP_L	2.02	2.57	1.76	165
46	PP_L	2.62	2.68	2.30	161
47	PP_L	2.99	4.92	2.54	157
48	PP_L	3.32	4.72	3.53	150
49	PP_H	1.56	1.07	1.17	166
50	PP_H	1.82	1.94	1.86	162.5
51	PP_H	2.97	2.15	2.04	160
52	PP_H	3.22	2.76	2.05	158
53	PP_H	3.17	3.50	2.16	158
54	PP_H	3.38	4.08	3.30	151
55	HF_L	2.54	2.66	3.12	162.5
56	HF_L	3.58	4.67	3.50	157.5
57	HF_L	4.13	5.40	4.58	155
58	HF_L	6.84	8.96	8.43	150
59	HF_L	11.23	14.85	12.76	140
60	HF_L	18.36	26.39	20.19	140

61	HF_M	4.88	3.46	3.77	157.5
62	HF_M	4.89	5.63	4.71	152.5
63	HF_M	6.44	7.15	5.46	152.5
64	HF_M	6.94	7.68	6.49	150
65	HF_M	9.76	11.10	9.09	147.5
66	HF_M	15.36	18.53	12.59	140

923